Main Manuscript for

SLC35G3 is a UDP-N-acetylglucosamine transporter for sperm glycoprotein formation and underpins male fertility in mice

Authors:

Daisuke Mashiko[1,2], Shingo Tonai[1], Haruhiko Miyata[1], Martin M. Matzuk[3,4], and *Masahito Ikawa[1, 2, 5, 6,7]

Affiliation:

1. Department of Experimental Genome Research, Research Institute for Microbial Diseases, Osaka University, Suita, Osaka 565-0871, Japan;
2. Immunology Frontier Research Center, Osaka University, Suita, Osaka 565-0871, Japan
3. Department of Pathology and Immunology, Baylor College of Medicine, Houston, TX 77030.
4. Center for Drug Discovery, Baylor College of Medicine, Houston, TX 77030.
5. Center for Advanced Modalities and Drug Delivery System, Osaka University, Osaka 565-0871, Japan
6. Center for Infectious Disease Education and Research, Osaka University, Osaka 565-0871, Japan
7. The Institute of Medical Science, The University of Tokyo, Minato-ku, Tokyo 108-8639, Japan.

***Corresponding author. Email: ikawa@biken.osaka-u.ac.jp**

Author Contributions: Conceptualization: DM, MMM, and MI. Data curation: DM. Formal analysis: DM. Funding acquisition: HM, MMM and MI. Methodology: DM, HM, MMM, and MI. Project administration: MI. Investigation: DM, ST, HM, and MI. Visualization: DM, HM, and MMM. Supervision: MI. Writing—original draft: DM and MI. Writing—review & editing: All authors

Competing Interest Statement: The authors declare no conflict of interest.

Classification: Biological Sciences, Developmental Biology.

Keywords: Zona pellucida binding, Utero tubal junction penetration, Sterility

This file includes:

Main Text

Figures 1 to 7

Abstract

Despite the recognized importance of glycans in biological phenomena, their complex roles in spermatogenesis and sperm function remain unclear. SLC35G3, a 10-transmembrane protein specifically found in early round spermatids, belongs to the sugar-nucleotide transporter family, indicating its involvement in glycan formation. In this study, we found that *Slc35g3* knockout male mice were sterile due to impaired sperm functions in uterotubal junction passage, zona pellucida binding, and oocyte fusion. Mouse SLC35G3 has UDP-GlcNAc transporter activity, and its ablation caused abnormal processing of the sperm plasma membrane and acrosome membrane proteins. Reported human *SLC35G3* mutations (F267L and T179HfsTer27) diminished the UDP-GlcNAc transporter activity of SLC35G3, implying infertility risks in males carrying these mutations. Our findings unveil the vital roles of SLC35G3 in the glycan formation of sperm membrane proteins critical for sperm fertilizing ability.

Introduction

Glycosylation is a post-translational modification that ensures target protein synthesis, secretion, stability, characterization, and/or function (1-3). In the endoplasmic reticulum (ER), the oligosaccharyltransferase complex (OSTC) co-translationally transfers core glycans assembled on dolichol phosphate to asparagine residues of nascent proteins. Subsequently, these proteins undergo a quality control process in which the core glycan structure is processed by glucosidases, resulting in a monoglucosylated form that binds to ER lectin chaperones, calnexin (CANX) and calreticulin (CALR). Once disulfide bonds are correctly formed by protein disulfide isomerase (PDI) and the protein is properly folded, the protein is transported to the Golgi (4, 5). Notably, there are testis-specific proteins that are required for these processes and the regulation of sperm fertilizing ability. Recent studies suggest that FREY tightly interacts with proteins involved in N-glycosylation, and its disruption destabilizes OSTC and causes subsequent ablation of the acrosomal membrane proteins essential for sperm-egg fusion (6, 7). In addition to the CANX/CALR/PDI complex in somatic cells, their testis-specific paralogs, CLGN/CALR3/PDILT, are required for ADAM3 sperm membrane glycoprotein maturation to equip sperm fertilization competence, including the ability to pass through the uterotubal junction (UTJ) (8). In the ER to Golgi secretory pathway, more than 200 glycosyltransferases, such as mannosyl (alpha-1,3-)-glycoprotein beta-1,2-N-acetylglucosaminyltransferase (MGAT) and N-acetylgalactosaminyltransferase (GALNT), add further diversity by conferring various properties, such as solubility and adhesiveness to the proteins. Once glycoproteins reach the cell surface, some are secreted to form the extracellular matrix, while others remain and contribute to cell adhesion and interactions with substrates or other cells. Among these glycosyltransferase-like proteins, DPY19L2 (a probable C-mannosyltransferase), MGAT4D, MGAT4E, MGAT4F, and GALNTL5 show testis-specific expression by *in silico* analysis (9). *Dpy19l2* knockout mice are infertile due to globozoospermia (10) and mutation in *Galntl5* resulted in asthenozoospermia (11). Of note, GALNTL5 does not exhibit transferase activity *in vitro* (12). While *Mgat4d* knockout mice are fertile (13), *Mgat4e* and *Mgat4f* orthologs do not exist in humans, and their knockout mice need to be generated to reveal if they have indispensable or redundant functions in mice. Collectively, these findings suggest that the spermatogenic cells have a unique system for the production and quality control of

glycoproteins and some of them are critical for spermatogenesis, sperm functions, and male fertility.

In the present study, we focused on the solute carrier (SLC) 35 family of nucleotide sugar transporters, which are responsible for importing sugars that serve as substrates for glycosyltransferases. Sugars are conjugated to nucleotides and transported by specific SLC35 family antiporters into the ER and Golgi apparatus, where glycosyltransferases utilize them to modify target proteins. Glycan structures are synthesized from sugars including D-glucose (Glc), D-galactose (Gal), N-acetyl-D-glucosamine (GlcNAc), N-acetyl-D-galactosamine (GalNAc), L-fucose (Fuc), D-glucuronic acid (GlcA), D-mannose (Man), N-acetylneuraminic acid (Neu), and D-xylose (Xyl). Among the SLC35 paralogs, SLC35A1 transports CMP-Sialic Acid, SLC35A2 transports UDP-Gal, SLC35B4 transports UDP-GlcNAc, and SLC35C1 transports GDP-Fuc (14). Of the 27 SLC35 family members, most show ubiquitous expressions, including in spermatogenic cells. Notably, in silico analysis revealed that *Slc35g3* is the only SLC35 family member specifically expressed in the testis. *Slc35g3* emerged in amphibians and is conserved in primates. We elucidated the biochemical properties of SLC35G3 *in vitro* and generated *Slc35g3* knockout mice to study its physiological functions *in vivo*. We discovered that SLC35G3 is a spermatogenic cell-specific UDP-GlcNAc transporter, and *Slc35g3* ablation results in abnormal processing of sperm plasma membrane and acrosome membrane glycoproteins required for sperm fertilizing ability and male fertility.

Results

SLC35G3 is expressed during late spermatogenesis and localized in the Golgi apparatus

In mice, *Slc35g3* comprises two coding exons and is located on chromosome 11, whereas it is located on chromosome 17 in humans. The TreeFam (15) data confirmed the evolutional conservation of *Slc35g3* among vertebrates (**Fig. 1A**). RT-PCR analysis indicates that it is prominently expressed in the testis, beginning 21 days postpartum (**Fig. 1B**), suggesting expression from the secondary spermatocyte stage to the round spermatid stage in mice. The Mammalian Reproductive Genetics Database (16) revealed that *Slc35g3* is the only mouse SLC35 family that shows a testis-specific transcription pattern (**Fig. S1**). A previous scRNA-seq analysis suggested that transcription of *Slc35g3* initiates in round spermatids (**Fig. 1C;** Mouse Cell Atlas; 17). Both AlphaFold2 (18) and TOPCONS (19) analyses supported that SLC35G3 has 10 transmembrane domains (**Fig. 1D**) likely forming a homodimer (**Fig. S2**). Immunostaining colocalizes SLC35G3 with Golgi marker (GM) 130 (Golgin A2), indicating SLC35G3 localization in the Golgi of mouse testicular germ cells (**Fig. 1E**).

Slc35g3$^{-/-}$ mice showed male infertility

To investigate the roles of *Slc35g3* in male reproduction, we used CRISPR/Cas9 to generate a homozygous knockout mouse line (*Slc35g3*$^{-/-}$) with an 1804-bp deletion on a hybrid B6D2 background. This deletion resulted in the loss of the entire *Slc35g3* coding region (**Fig. 2A, 2B**), indicating that it should be a null allele.

Slc35g3$^{-/-}$ mice exhibit grossly normal development, appearance, and behavior, consistent with its testis-restricted expression. Absence of the *Slc35g3* mRNA and SLC35G3 protein in the *Slc35g3*$^{-/-}$ testes was verified by RNA-seq (**Fig. S3)** and western blot analysis (**Fig. 2C**), respectively. The specific expression of SLC35G3 in the testis, but not in epididymal sperm, suggests that its function is restricted to spermatogenesis. Moreover, immunofluorescence of SLC35G3 confirmed its absence in the Golgi of *Slc35g3*$^{-/-}$ mice (**Fig. S4**). Testes of *Slc35g3*$^{-/-}$ male mice appeared normal in both appearance and weight (**Fig. 2D, 2E;** +/+ vs. -/-, two-sided Student's t-test; $\boldsymbol{P}$ = 0.42). Despite successful copulation, as evidenced by the presence of vaginal plugs, *Slc35g3*$^{-/-}$ male mice are sterile (**Fig. 2F;** +/+ vs. -/-, two-sided Wilcoxon rank-sum test, $\boldsymbol{P} = 2.87 \times 10^{-10}$). Examination of seminiferous tubule and epididymis sections revealed no overt abnormalities **(Fig. 2G** and **Fig. S5**). Furthermore, computer-assisted sperm analysis revealed no significant differences in the motility of sperm from control and *Slc35g3*$^{-/-}$ males (**Fig. S6**).

Slc35g3$^{-/-}$ -derived sperm exhibit abnormal head morphology

Given the subtle morphological changes observed in *Slc35g3*$^{-/-}$-derived sperm (**Fig. 3A**), we employed elliptic Fourier descriptors (20, 21) to characterize the entire sperm head shape and conducted a principal component (PC) analysis (**Fig. 3B, 3C, 3D**). Wild-type-derived sperm and *Slc35g3*$^{-/-}$-derived sperm could be differentiated based on their PC2 analysis of the tip of the sperm heads, with *Slc35g3*$^{-/-}$-derived sperm displaying a relatively higher PC2 value (**Fig. 3C**), indicating the lack of the hook shape in *Slc35g3*$^{-/-}$ -derived sperm. The head shape of *Slc35g3*$^{-/-}$-derived sperm resembled that of sperm from *Fam71f2*$^{-/-}$ (recently renamed as *Garin1a*, Golgi-associated RAB2 interactor 1A)(22) mice (**Fig. S7**). However, *Slc35g3*$^{-/-}$ mice exhibited a more severe fertility phenotype compared to *Fam71f2*$^{-/-}$ mice (average litter size = 0 and 4.4 pups/litter, respectively), suggesting that sperm head morphology is not the sole cause of sterility in *Slc35g3*$^{-/-}$ mice.

Slc35g3$^{-/-}$-derived sperm exhibit impaired zona pellucida (ZP) binding and fertilization

To further analyze the cause of infertility in *Slc35g3* null male mice, we performed an in vitro fertilization (IVF) assay. We first performed conventional IVF using cumulus-intact oocytes with 2×10^5 sperm/mL insemination and found no oocytes fertilized with spermatozoa from *Slc35g3*$^{-/-}$ males (**Fig. 4A**). By removing cumulus cells followed by insemination (**Fig. 4B**), we found a decline in the number of *Slc35g3*$^{-/-}$-derived spermatozoa bound to the ZP (**Fig. 4C, 4D**), no oocytes fertilized as well (**Fig. 4E,** Wilcoxon rank-sum test; $\boldsymbol{P}$ = 0.0079). Further study, using ZP-free oocytes preloaded with Hoechst33342 (**Fig. 4F**), revealed a significantly lower number of sperm fusing the oocyte compared to control *Slc35g3*$^{+/-}$ (**Fig. 4G, H**, +/- vs. -/-, Wilcoxon rank-sum test, $\boldsymbol{P} = 1.71 \times 10^{-21}$). Notably, oolemma fusion and fertilization were improved with a 10 times higher sperm concentration from *Slc35g3*$^{-/-}$ males but were still significantly decreased compared to the lower concentrations of sperm from controls（**Fig. S8)**. Lastly, IVF

performed using cumulus-intact oocytes with 10 times more sperm insemination (2×10^6 sperm/mL) resulted in a reduced fertilization rate (45.7%, 21/46), but we succeeded in obtaining 10 live pups from these fertilized eggs (**Fig. S9**). Our results indicate that *Slc35g3*$^{-/-}$-derived sperm have defects in ZP binding and oolemma fusion ability but genomic integrity is intact.

Slc35g3-deficient mice show impaired sperm migration to the oviduct.

As spermatozoa lacking ZP binding frequently cannot pass through the uterotubal junction (UTJ) and reach the oviduct (8), we observed sperm UTJ passage after mating. This observation was facilitated by a red fluorescence signal in the sperm tails from Tg mice (CAG/*su9*-DsRed2, *Acr3*-eGFP) (23; **Fig. 5A**). Two hours after copulation with wild-type female mice (**Fig. 5B**), control *Slc35g3*$^{+/-}$-derived sperm tail signals marked by red fluorescence were observed within the oviduct (**Fig. 5C**). In contrast, *Slc35g3*$^{-/-}$-derived sperm were found in the uterus but not in the oviduct (**Fig. 5C**). Thus, male infertility of *Slc35g3*$^{-/-}$ mice was likely caused primarily by impaired sperm passage through the UTJ.

Slc35g3 absence causes a reduced amount and abnormal processing of sperm glycoproteins.

To understand the molecular mechanisms behind the disrupted sperm functions of *Slc35g3*$^{-/-}$ mice, we analyzed glycoproteins related to each process. First, we examined proteins involved in acrosome formation. Immunoblot analysis of *Slc35g3*$^{+/+}$ and *Slc35g3*$^{-/-}$ testis lysates showed a reduction in the amount of ZP binding protein 1 (ZPBP1; 24), whereas Golgi-associated PDZ and coiled-coil motif containing (GOPC; 25) levels remained unchanged (**Fig. 6A**). Interestingly, some bands of sperm acrosome associated 1 (SPACA1; 26) disappeared in *Slc35g3*$^{-/-}$ testis lysates. SPACA1 is N-glycosylated, and treatment of testis and caudal sperm lysates with peptide-N-glycosidase F (PNGase F; **Fig. 6B, Fig. 6C**) resulted in comparable SPACA1 band patterns between *Slc35g3*$^{+/+}$ and *Slc35g3*$^{-/-}$ testes but not in sperm lysates. A similar result was also reported in *Fam71f1*$^{-/-}$ (Garin1b; 22) mice, which exhibit abnormal acrosome formation.

Next, we examined proteins involved in ZP binding. Levels of a disintegrin and metalloprotease (ADAM) 1B (27) were comparable between *Slc35g3*$^{+/-}$ and *Slc35g3*$^{-/-}$ in the testis (**Fig. 6D**) and sperm (**Fig. 6E**). Levels of CKLF-like MARVEL transmembrane domain containing (CMTM) 2A and CMTM2B (28) were reduced in *Slc35g3*$^{-/-}$ testis lysates but not in sperm. The expression pattern of ADAM3 (29, 30) was comparable between *Slc35g3*$^{+/-}$ and *Slc35g3*$^{-/-}$ testis, yet the amount of a smaller isoform was elevated in *Slc35g3*$^{-/-}$-derived sperm lysates, indicating aberrant processing. After PNGaseF treatment of proteins, the ADAM3 band pattern was comparable between *Slc35g3*$^{+/-}$ and *Slc35g3*$^{-/-}$ (**Fig. S10**). Given the aberrant ADAM3 band pattern was also observed in testis expressed gene 101 (TEX101) knockout (31) epididymal caput sperm, we examined TEX101 levels through western blot analysis; however, the amount of TEX101 was comparable between *Slc35g3*$^{+/-}$ and *Slc35g3*$^{-/-}$ testis lysates (**Fig. 6D**). Given that the testicular *Ace*$^{-/-}$ (t-ACE; 32, 33, 34) caused aberrant localization of ADAM3, we examined t-ACE levels through western blot analysis and found that the amount of t-ACE was comparable between *Slc35g3*$^{+/-}$ and *Slc35g3*$^{-/-}$ in both testis and sperm lysates

(**Fig. 6D, 6E**). In the previous studies, lymphocyte antigen 6 family member K (*Ly6k*)$^{-/-}$ (35), *Spaca4*$^{-/-}$ (36), and LY6/PLAUR Domain Containing 4 (*Lypd4*)$^{-/-}$ (37) sperm showed impaired ZP binding; however, the amount of ADAM3 remained normal. The amount of LY6K was reduced in *Slc35g3*$^{-/-}$ testis lysates (**Fig. 6D**) and the amount of SPACA4 was comparable between *Slc35g3*$^{+/-}$ and *Slc35g3*$^{-/-}$ in both testis and sperm lysates (**Fig. 6D, 6E**). However, the amount of LYPD4 in *Slc35g3*$^{-/-}$ testis lysates decreased, and the lower molecular weight band disappeared in *Slc35g3*$^{-/-}$-derived sperm lysates (**Fig. 6E**), indicating the occurrence of a protein processing error or another non-N-linked oligosaccharide post-translational defect.

Finally, we focused on the inner acrosomal membrane proteins involved in oolemma fusion. IZUMO1 is an N-glycosylated acrosome membrane protein, and the first to be identified as essential for sperm-oolemma fusion using knockout mice (38). The levels of IZUMO1 decreased in both the testis and sperm of *Slc35g3*$^{-/-}$ mice. Although the amount of IZUMO1 in sperm was less, we did not see any other bands in the western blot analysis. IZUMO1 could relocate to the equatorial segment where fusion occurs after the acrosome reaction in *Slc35g3*$^{-/-}$ derived spermatozoa (**Fig. S11**). Equatorin (EQTN) is an O-linked glycosylated protein on the inner acrosomal membrane, not essential for oolemma fusion but rather functions in oolemma binding. The EQTN signal showed no difference between *Slc35g3*$^{+/-}$ and *Slc35g3*$^{-/-}$ testes, but it disappeared in *Slc35g3*$^{-/-}$-derived sperm. Intriguingly, mass spectrometry analysis of sperm lysates showed comparable quantitative values of EQTN between *Slc35g3*$^{+/-}$ and *Slc35g3*$^{-/-}$ mice (**Table S1**). With the fact that the anti-EQTN antibody MN9 recognizes both peptide and glycan structures and that the glycan structure (39), our data suggests that EQTN glycosylation is aberrant in *Slc35g3*$^{-/-}$-derived sperm. SPACA6 is known to be lost from all the sperm-oolemma fusion defective sperm (i.e., *Dcst1/2*, *Fimp*, *Izumo1*, *Sof1*, *Spaca6*, and *Tmem95* knockout models) (40); however, we did not see any difference in the intensity and band pattern using western blot analysis.

Slc35g3$^{-/-}$-derived spermatozoa show impaired glycan structures

To analyze the protein glycosylation status during spermatogenesis, we performed lectin blot analyses using testis lysates (**Fig.7A**). The band patterns of concanavalin A (ConA; detecting mannose), *Aleuria aurantia* lectin (AAL; detecting fucose), and *Maackia amurensis* II (MAL-II; detecting sialic acid + core1 structure) were comparable between *Slc35g3*$^{+/+}$ and *Slc35g3*$^{-/-}$ samples. Notably, with PNA which detects galactose β1-3 acetyl galactosamine (core 1 structure), the intensity of a band around 60 kDa increased in *Slc35g3*$^{-/-}$ testis. As PNA binding is known to be inhibited by any galactose modifications (41), the core 1 modifications might be disrupted in the target protein. With *Laetiporus sulphureus* lectin N-terminal domain (LSL-N; detecting LacNAc: galactose-GlcNAc), signal intensities for small proteins decreased. Intriguingly, the difference became evident when we performed lectin blot analysis using mature spermatozoa. Some major signals disappeared in PNA and LSL-N blot analysis (**Fig. 7B**).

Mouse (m) *Slc35g3* overexpression restored glycan levels in HEK293T cells without human (h) *SLC35B4*

To investigate whether SLC35G3 acts as a UDP-GlcNAc transporter, we performed rescue experiments with HEK293T cells. First, we designed two gRNAs to knock out *hSLC35B4* encoding a known UDP-N-acetylglucosamine (UDP-GlcNAc) transporter that is highly expressed in HEK293T cells (**Fig. S12A**). The *hSLC35B4* knockout cells were obtained by transfecting pX459 containing two gRNAs and puromycin-resistant cassette, followed by puromycin treatment (**Fig. S12B**). After three passages, the cells were transfected with a plasmid expressing *mSlc35b2* (encoding a phosphoadenosine phosphosulfate transporter), *mSlc35b4*, or *mSlc35g3*-mCherry. We found that the introduction of *mSlc35b2* did not rescue the amounts of proteins with GlcNAc modification (**Fig. 7C**). Conversely, transfection with the *mSlc35b4*-expressing plasmid rescued GlcNAc modification levels. Further, the LSL-N signals were rescued by *mSlc35g3* transfection (**Fig. 7C**), suggesting that mSLC35G3 functions as a UDP-GlcNAc transporter.

T179HfsTer27 and F267L mutants failed to rescue glycan loss in *hSLC35B4*-disrupted cells

Among the frameshift mutations found in human genomes (n= 76156, gnomAD; 42), T179HfsTer27 frame mutation has a relatively high allele frequency ($1.88e^{-3}$), and homozygous mutations are observed in 54 individuals (29 females and 25 males). Moreover, AlphaMissense (43), a deep learning model trained on protein sequences and annotations of pathogenicity, predicted 35 pathogenic missense mutations in the *hSLC35G3* gene. Among these, two mutations (F215L and F267L) were identified in human genomes, and we focused on F267L, which showed potential detrimental effects according to the evolutionary conservation and protein 3D structure (PolyPhen-2; 44). PCR and subsequent direct sequencing confirmed that the *hSLC35G3* expression plasmid (wild-type, FS, or F267L) was introduced into *hSLC35B4*$^{-/-}$ cells. With lectin blot analysis using LSL-N, the signal decreased by *hSLC35B4*$^{-/-}$ was rescued by the introduction of wild-type *hSLC35G3*, while no signal recovery was observed upon the introduction of FS or F267L (**Fig. 7D**). The band patterns of ConA modification remained consistent across all transfected cells. These findings suggest a loss of function in the T179HfsTer27 and F267L mutations.

Discussion

In this study, we identified SLC35G3 as a testis-specific UDP-GlcNAc transporter to underpin proper sperm glycoprotein synthesis and functions. Although *Slc35g3*$^{-/-}$ male mice are viable, healthy, and produce motile sperm, they are completely infertile, revealing a critical and unique role of SLC35G3 for producing functional spermatozoa and male fertility. In vitro studies further implicated latent male infertility due to *SLC35G3* mutations.

During spermatogenesis, *Slc35b4* is expressed in earlier stages, but it decreases and is replaced by *Slc35g3* in later stages (**Fig. S1**). The reason for the stage-dependent usage of two transporters is unknown, but it may be related to the formation of acrosomes, which are rich in glycosylated proteins, in the later stages of spermatogenesis.

Although our in vitro data showed no clear differences (**Fig.7C**), SLC35B4 and SLC35G3 may have different activities and/or functions. Alternatively, SLC35G3 may have a lower optimal temperature because spermatogenesis progresses at a lower temperature (45). Considering the transcript level of *Slc35g3* in later spermatogenesis stages (highest TPM=320 at round spermatid) is higher than that of *Slc35b4* in the earlier stage (highest TPM=21 at spermatogonia), spermatids may simply require more UDP-GlcNAc transporter activity. Further in vitro and in vivo studies will be needed to answer these questions, including transgenic mice expressing *Slc35b4* under the *Slc35g3* promoter and vice versa. The answer will also help us to understand why and how spermatogenic cells require a certain number of paralogous genes to be expressed specifically.

Lectin blot analyses revealed no differences in ConA signals targeting terminal mannose (**Fig. 7B**), indicating the normal formation of high-mannose-type oligosaccharides for N-glycan biosynthesis in the ER of *Slc35g3*$^{-/-}$ spermatogenic cells (46). For O-glycans, there was an increase in PNA signals (core 1, Gal-GalNAc) and a reduction in LSL-N signals (LacNAc: Gal-GlcNAc), while no changes were observed for MAL-II (sialic acid) and AAL (fucose). These findings suggest that SLC35G3 plays a more important role in glycan elongation rather than core structure, and the impaired elongated glycan structure affected the properties of glycoproteins and following sperm morphology and functions in *Slc35g3*$^{-/-}$ mice.

While spermatogenesis looked grossly normal in *Slc35g3*$^{-/-}$ mice (**Fig. 2D, 2E, and 2G, fig. S6**), their spermatozoa displayed multiple phenotypic abnormalities in head morphology (**Fig. 3**), UTJ migration (**Fig. 5**), and fertilization (**Fig. 4**). Regarding sperm head malformation, while globozoospermia results in male infertility (e.g., *Zpbp1* (24), *Gopc* (25), and *Spaca1* (26) knockout mice), most of the knockout mice with only subtle head malformation can produce offspring, although at lower levels (e.g., *Zpbp2* (24), *Fam71f2* (22), and *Garin2-Garin5* (47) knockout mice). We found a subtle sperm head malformation in *Slc35g3*$^{-/-}$ mice, but it should not be underestimated. For example, it has been shown that mutations in multiple genes synergistically worsen head morphology, even in the heterozygous state (48). Although we are still far from unraveling these molecular interactions, we have revealed the importance of SLC35G3-mediated UDP-GlcNAc transport for ZPBP1 stabilization and SPACA1 processing. Further research is warranted on individual molecules and specific glycans to better understand their relationship during sperm head morphogenesis.

Slc35g3$^{-/-}$-derived spermatozoa exhibited defective UTJ passage (**Fig. 5**) and ZP binding (**Fig. 4D**). These defects are commonly linked and observed in many infertile knockout mice, and ADAM3 is absent from most of these knockout spermatozoa (37, 49). However, ADAM3 is present in the *Slc35g3*$^{-/-}$-derived spermatozoa as in four other knockout mouse lines that show the same phenotype (i.e., *Ly6k, Pgap1, Spaca4,* and *Lypd4* knockout lines). These results suggest that ADAM3 may be dysfunctional in these mutant sperm, or that there may be an unknown factor responsible for UTJ passage and ZP binding. Because LY6K and PGAP1 only function in the testis and disappear from mature spermatozoa, so we analyzed the presence of LYPD4 and SPACA4 in mature spermatozoa and found that, there was abnormal processing of LYPD4 in *Slc35g3*$^{-/-}$-derived spermatozoa (**Fig. 6E**) compared to WT sperm (50). Since ADAM3 is no longer active in humans, more attention needs to be paid to LYPD4 to understand the sperm fertilizing ability.

We next focused on the inner acrosomal membrane proteins because *Slc35g3*$^{-/-}$ derived spermatozoa were defective in fusing with oocytes (**Fig. 6D, 6E**). While we did

not see any differences in SPACA6 western blot analysis, we found a decrease of IZUMO1 in *Slc35g3*$^{-/-}$-derived spermatozoa, which is consistent with our previous study showing the lack of glycosylation accompanied by a decrease in IZUMO1 levels and a reduction in the number of pups (51). Intriguingly, while EQTN was detected by MS analysis (**Table S1**), signals disappeared in our western blot analysis using an antibody recognizing EQTN O-glycans (37; **Fig. 6E**), suggesting the presence of EQTN protein without O-glycans. As *Eqtn* knockout spermatozoa decreased their oolemma binding ability (37), EQTN glycans may directly contribute to oolemma binding. These results suggest that SLC35G3 regulates sperm-oolemma fusion through O-linked glycosylation of inner acrosomal membrane proteins.

Finally, we examined mutations in human *SLC35G3* for their potential risk of male infertility. An in vitro study revealed that the T179HfsTer27 (17-35193772-GT-G) mutation lost sugar-nucleotide transporter activity. According to gnomAD, its frequency is 1.88×10^{-3} and 54 individuals have been identified as homozygous. In addition, the observed/expected ratio of single nucleotide variants causing loss of function was 0.53, suggesting the presence of selective pressure due to mutations. Assessment of their sperm fertilizing ability would be beneficial to understanding glycosylated protein synthesis and functions in human spermatozoa. Even if the mutation caused male infertility, as we obtained healthy offspring by IVF with higher concentration sperm insemination, intracytoplasmic sperm injection might not be necessary for their treatment.

In conclusion, our research suggests that SLC35G3 functions as a testis-specific UDP-GlcNAc transporter during late spermatogenesis. We reaffirmed that glycosylation-related genes specific to the testis play a crucial role in the synthesis, quality control, and function of glycoproteins on sperm, which are essential for male fertility through their interactions with eggs and the female reproductive system. Furthermore, we demonstrated that human SLC35G3 also exhibits transporter activity, and proposed a loss of function mutations that may cause male infertility. Further research on this gene and sperm glycoprotein synthesis has the potential to contribute to understanding the causes of male infertility, developing treatments, and advancing contraceptive methods.

Methods

Experimental design

In this study, we developed an integrated approach, combining *in silico* analysis with experimental techniques, to elucidate the functions of SLC35G3. To generate *Slc35g3* knockout (*Slc35g3*$^{-/-}$) male mice, we used the CRISPR/Cas9 system and conducted *in silico* analysis for off-target/cleavage activity. Male fertility assessment encompasses mating with females, alongside IVF assays. Based on the preliminary literature on the SLC35 family, SLC35G3 is hypothesized to be a nucleotide sugar transporter. Therefore, we performed lectin blot analysis using tissue lysate/HEK293T cell lysate.

Animals

The manuscript adhered to the ARRIVE guidelines 2.0 for reporting. This study was performed following the standards outlined in the Guide for the Care and Use of Laboratory Animals. All animal experiments were approved by the Animal Care and Use Committee of the Research Institute for Microbial Diseases at Osaka University, Osaka, Japan (#Biken-AP-H30-01). The mice used in the study were sourced from Japan SLC,

Inc. (Shizuoka, JP) and were bred under specific pathogen-free conditions. They were housed at 23°C, with a relative humidity of 50%, and a 12-h dark/12-h light cycle, with unrestricted access to water and commercial food pellets *ad libitum*. All genetically modified mice produced in this study will be accessible through either the RIKEN BioResource Research Center in Ibaraki, Japan, or the Center for Animal Resources and Development (CARD) at Kumamoto University, Japan.

***In silico* analysis**

Phylogenetic tree analysis was performed using TreeFam (15; http://www.treefam.org/), while the Mammalian Reproductive Genetics Database (16; https://orit.research.bcm.edu/MRGDv2) was used for mRNA expression analysis of the SLC35 family. Previously reported single-cell RNA sequencing data (17; https://bis.zju.edu.cn/MCA/) were employed to analyze *Slc35g3* mRNA expression in testicular germ cells. The AlphaFold database (18; https://alphafold.ebi.ac.uk/) was utilized for structure prediction, and TOPCONS (19; https://topcons.cbr.su.se/) was employed for the topological analysis of SLC35G3.

RNA isolation and reverse transcription polymerase chain reaction

RNA was extracted and purified from various adult tissues of C57BL/6N mice at different stages using TRIzol reagent (Cat. No. 15596018, Thermo Fisher Scientific, Waltham, MA, USA), according to the manufacturer's instructions. Reverse transcription was conducted with the RNA using the SuperScript III First-Strand Synthesis System (Cat. No. 18080051; Thermo Fisher Scientific). PCR amplification was performed using a KOD Fx Neo (KFX-201; TOYOBO Co., LTD, Osaka, JP). The primer sequences used for each gene are listed in **Table S2**.

Visualization using fluorescence

Preparation of spermatogenic cells was performed as previously described for testicular cells (52). Briefly, the seminiferous tubules were cut into small pieces, and the contents were extracted by pressing them against a coverslip and frozen. Hoechst33342 (H3570, Thermo Fisher Scientific) and Alexa Fluor 568-conjugated peanut agglutinin (PNA; L32458, Thermo Fisher Scientific) were used to stain the nuclei and acrosomes of cauda epididymal spermatozoa. Observations were performed using a fluorescence microscope (BX53; Olympus, Tokyo, JP).

Generation of *Slc35g3* knockout mice

Slc35g3 knockout mice were generated using the CRISPR/Cas9 system. Guide RNA design and potential off-target analysis were performed using the software programs CRISPRdirect (https://crispr.dbcls.jp/) and CRISPOR (https://crispor.tefor.net/). Fertilized eggs were obtained from the oviducts of super-ovulated B6D2F1 females, which were then mated with BDF1 males. Ribonucleoprotein (RNP) complexes, comprising synthesized CRISPR RNA (crRNA), trans-activating crRNA (tracrRNA), and CAS9 protein, were introduced into fertilized eggs using a NEPA21 super electroporator (Nepa Gene Co., Ltd, Chiba, JP). The treated eggs were cultured in potassium simplex optimization medium containing amino acids (KSOMaa) until the two-cell stage and were subsequently transplanted into the oviducts of 0.5-day pseudopregnant ICR females. The identity of the pups was confirmed by PCR and Sanger sequencing. Guide RNA and primer sequences are listed in **Table S2**.

In vivo male fertility test

Each 8-week-old male, carrying either the *Slc35g3* wild-type or mutated gene, was individually housed with three 8-week-old B6D2F1 female mice for 2 months. Daily observations were made to identify mating plugs, and the number of resultant pups was recorded. A minimum of three males were included in each experimental group for statistical analysis.

Histological analysis of testis

Testes were dissected, fixed in Bouin's fluid (Polysciences, Warrington, PA, USA), and embedded in paraffin wax. Subsequently, 5-µm-thick sections were obtained from the paraffin blocks using a Microm HM325 microtome (Microm, Walldorf, DE, Germany). The sections were sequentially dehydrated with xylene and ethanol, followed by a 15-minute incubation in a 1% periodic acid solution. After washing under running water for 15 min, the sections were treated with Schiff's reagent (FUJIFILM Wako, Osaka, JP) for 30 min and then stained with Mayer's hematoxylin solution for 3 min after an additional 15-min wash. Following these processes, the stained samples were observed using SLIDEVIEW VS200 (Olympus, Tokyo, JP).

Morphological analysis of sperm

Elliptical Fourier transform analysis was performed as previously described (20, 21). Briefly, photographs of the spermatozoa were captured using a microscope equipped with a complementary metal oxide semiconductor (CMOS) camera (BX53, DP74, Olympus). The sperm head shape was manually tracked from the photographs, and the elliptic Fourier analysis was performed using Momocs, a contour analysis package of the statistical analysis software R x64 4.1.2(https://www.r-project.org/). Top PC1-3 scores were visualized using a custom Python code.

In vitro fertilization

In vitro fertilization was performed according to the previously established procedures (7). Cauda epididymal spermatozoa were dispersed in a drop of Toyoda, Yokoyama, Hoshi (TYH) medium (53) covered with paraffin oil (26117-45, Nacalai Tesque Inc., Kyoto, JP) for 2 h at 37°C under 5% CO_2 to facilitate capacitation. Eggs obtained from the oviducts of superovulated females were placed in TYH drops. Cumulus cells were removed by treating the oocytes with 330 µg/mL of hyaluronidase (FUJIFILM Wako Pure Chemical Corp., Osaka, JP) for 5 min. To eliminate the ZP, eggs were treated with 1 mg/mL collagenase (C1639, Merck KGaA, Darmstadt, DE, Germany) for 5 min. The capacitated spermatozoa were introduced into a drop containing cumulus-intact, cumulus-free, or ZP-free eggs at a final concentration of 2×10^5 or 2×10^6 spermatozoa/mL. Pronuclei formation was observed 8 hours after insemination.

Computer-assisted sperm analysis

Sperm velocity was analyzed as previously described (54). Cauda epididymal spermatozoa were dispersed in 100 µL drops of TYH medium. Sperm motility parameters were measured using the CEROS II sperm analysis system (software version 1.4; Hamilton Thorne Inc., Beverly, MA, USA) at 10 min and 2 h after incubation at 37°C under 5% CO_2. More than 200 spermatozoa were analyzed from each male.

Assessment of sperm passage through the utero-tubal junction

The assay was performed as previously described (31). Briefly, B6D2F1 female mice were subjected to superovulation through intraperitoneal injection of 5 U of equine chorionic gonadotropin (CG), followed by an additional 5 U of human CG (hCG) 48 h later. After 12 h of hCG injection, superovulated females were placed in cages with test males and vaginal plug formation was monitored at 30-min intervals. Upon confirmation of plug formation, the males were separated from the females. After approximately 2 h of plug formation, the oviducts, along with the connecting portion of the uterus, were excised. These tissues were mounted on slides as whole specimens, covered with coverslips, and examined using fluorescence microscopy (BZ-X810; Keyence Corporation, Osaka, JP) to assess the presence of sperm containing the mitochondrial DsRed2 marker.

Plasmid construction

The cDNAs encoding *mSlc35g3*, *mSlc35b2*, and *mSlc35b4* were amplified from mouse testis (C57BL/6N), whereas the cDNA encoding *hSLC35G3* was amplified from a human testis cDNA template (Quick Clone#637209, Takara Bio USA Inc., San Jose, CA, USA). The T179HfsTer27 and F267L cDNA mutants were generated using the *hSLC35G3* amplicon with the KOD Plus Mutagenesis Kit (SMK-101, TOYOBO Co. LTD, Osaka, JP) following the manufacturer's protocol. The *mSlc35g3* cDNA was inserted into the mCherry-tagged (C-terminus) pCAG vector, whereas the *mSlc35b2*, *mSlc35b4*, *hSLC35G3*, T179HfsTer27, and F267L cDNAs were cloned into the pCAG vector containing the CAG promoter and rabbit globin poly (A) signal, as previously described (55). The primers used to construct these plasmids are listed in Table S2.

Cell culture and transfection

HEK293T cells (56) were cultured in DMEM (11995–065, Thermo Fisher Scientific) supplemented with 10% fetal bovine serum (S1560, BioWest, Nuaillé, FR) and 1% penicillin-streptomycin-glutamine (10378–016, Thermo Fisher Scientific) at 37°C under 5% CO_2. Subsequently, these cells were transiently transfected with the plasmid DNA and cultured.

Western blot analysis/lectin blot analysis

Immunoblotting procedures closely followed those described previously (57). Testis, spermatozoa from the cauda epididymis, and collected cells were immersed in lysis buffer (1% Triton X-100, 50 mM Tris-HCl pH 7.5, 150 mM NaCl) supplemented with a protease inhibitor cocktail (Cat. No. 25955, Nacalai Tesque Inc.) and left to incubate overnight at 4°C. Subsequently, the lysate was centrifuged at 10 000 × *g* for 15 min at 4°C. The resulting supernatants were used for either lectin precipitation or SDS-PAGE for immunoblot or lectin blot analysis. PNGase F (P0704S, New England Biolabs Inc., Ipswich, MA, USA) was applied to the testis and sperm lysates to enzymatically treat the glycosidases, following the manufacturer's guidelines.

For lectin blot analysis, a blocking solution (10 mM Tris-HCl, 0.15 M NaCl, 0.05% Tween 20) was employed instead of skim milk for immunoblot analysis. The primary antibody was replaced with biotin-conjugated lectin, and the secondary antibody was substituted with HRP-conjugated streptavidin. The pertinent antibodies and lectins are listed in Table S3.

For lectin precipitation, supernatants from the testis were incubated with lectin-biotin overnight at 4°C, followed by incubation with streptavidin-conjugated Dynabeads (Cat. No. 65001, Thermo Fisher Scientific) for 1 h at room temperature. After three

washes with a mild buffer (42 mM Tris-HCl pH 7.5, 150 mM NaCl, 0.1% Triton X-100, and 10% glycerol), the complexes were eluted using a sample buffer containing 2-mercaptoethanol.

Mass spectrometry

The samples were subjected to mass spectrometry analysis as previously described (57). "The proteins were reduced with 10 mM dithiothreitol (DTT), followed by alkylation with 55 mM iodoacetamide, and digested in-gel by treatment with trypsin and purified with C18 tip (GL-Science, Tokyo, Japan). The resultant peptides were subjected to nanocapillary reversedphase LC-MS/MS analysis using a C18 column (25 cm × 75 um, 1.6 µm; IonOpticks, Victoria, Australia) on a nanoLC system (Bruker Daltoniks, Bremen, Germany) connected to a timsTOF Pro mass spectrometer (Bruker Daltoniks) and a modified nano-electrospray ion source (CaptiveSpray; Bruker Daltoniks). The mobile phase consisted of water containing 0.1% formic acid (solvent A) and acetonitrile containing 0.1% formic acid (solvent B). Linear gradient elution was carried out from 2% to 35% solvent B for 18 min at a flow rate of 400 nL/min. The ion spray voltage was set at 1.6 kV in the positive ion mode. Ions were collected in the trapped ion mobility spectrometry (TIMS) device over 100 ms and MS and MS/MS data were acquired over an m/z range of 100-1,700. During the collection of MS/MS data, the TIMS cycle was adjusted to 1.1 s and included 1 MS plus 10 parallel accumulation serial fragmentation (PASEF)-MS/MS scans, each containing on average 12 MS/MS spectra (>100 Hz), and nitrogen gas was used as collision gas." Protein identification was carried out using Mascot (version: 2.7.0; Matrix Science, London, UK) regarding Scaffold_4.10.0 (Proteome Software Inc., Portland, OR, USA). Human keratin peptides were excluded from the analysis.

Statistical analysis

Normality was assessed using the Shapiro–Wilk normality test, and variance was examined using the F-test. Non-parametric tests were performed using the Wilcoxon rank-sum test, whereas parametric tests were performed using the two-tailed Student's t-test or Welch's t-test. All statistical analyses were performed using R x64 4.1.2 (https://www.r-project.org/). Significance levels were established at *P<0.05, **P<0.01, and ***P<0.001. Data are presented as mean ± standard deviation (s.d.). Quantified data were visualized as dot plots using PlotsofData (58 https://huygens.science.uva.nl/PlotsOfData/) or custom Python code in Google Colab (https://colab.research.google.com/).

References

1. Matzuk, M.M. and Boime, I. The role of the asparagine-linked oligosaccharides of the a subunit in the secretion and assembly of human chorionic gonadotropin. J. Cell Biol. 106, 1049-1059 (1988).
2. Matzuk, M.M., Keene, J.L., and Boime, I. Site specificity of the chorionic gonadotropin N-linked oligosaccharides in signal transduction. J. Biol. Chem. 264, 2409-2414 (1989).

3. Schjoldager, K. T., Narimatsu, Y., Joshi, H. J., & Clausen, H. (2020). Global view of human protein glycosylation pathways and functions. *Nature reviews Molecular cell biology*, *21*(12), 729-749.

4. Tannous, A., Pisoni, G. B., Hebert, D. N., & Molinari, M. (2015, May). N-linked sugar-regulated protein folding and quality control in the ER. In *Seminars in cell & developmental biology* (Vol. 41, pp. 79-89). Academic Press.

5. Ikawa, M., Wada, I., Kominami, K., Watanabe, D., Toshimori, K., Nishimune, Y., & Okabe, M. (1997). The putative chaperone calmegin is required for sperm fertility. *Nature*, *387*(6633), 607-611.

6. Contreras, W., Wiesehöfer, C., Schreier, D., Leinung, N., Peche, P., Wennemuth, G., ... & Mentrup, T. (2022). C11orf94/Frey is a key regulator for male fertility by controlling Izumo1 complex assembly. *Science Advances*, *8*(31), eabo6049.

7. Lu, Y., Shimada, K., Tang, S., Zhang, J., Ogawa, Y., Noda, T., ... & Ikawa, M. (2023). 1700029I15Rik orchestrates the biosynthesis of acrosomal membrane proteins required for sperm–egg interaction. *Proceedings of the National Academy of Sciences*, *120*(8), e2207263120.

8. Tokuhiro, K., Ikawa, M., Benham, A. M., & Okabe, M. (2012). Protein disulfide isomerase homolog PDILT is required for quality control of sperm membrane protein ADAM3 and male fertility. *Proceedings of the National Academy of Sciences*, *109*(10), 3850-3855.

9. Oura, S., Mori, H., & Ikawa, M. (2022). Genome editing in mice and its application to the study of spermatogenesis. *Gene and Genome Editing*, *3*, 100014.

10. Pierre, V., Martinez, G., Coutton, C., Delaroche, J., Yassine, S., Novella, C., ... & Arnoult, C. (2012). Absence of Dpy19l2, a new inner nuclear membrane protein, causes globozoospermia in mice by preventing the anchoring of the acrosome to the nucleus. *Development*, *139*(16), 2955-2965.

11. Takasaki, N., Tachibana, K., Ogasawara, S., Matsuzaki, H., Hagiuda, J., Ishikawa, H., ... & Narimatsu, H. (2014). A heterozygous mutation of GALNTL5 affects male infertility with impairment of sperm motility. *Proceedings of the National Academy of Sciences*, *111*(3), 1120-1125.

12. Lu, Y., Oura, S., Matsumura, T., Oji, A., Sakurai, N., Fujihara, Y., ... & Ikawa, M. (2019). CRISPR/Cas9-mediated genome editing reveals 30 testis-enriched genes dispensable for male fertility in mice. *Biology of Reproduction*, *101*(2), 501-511.

13. Raman, J., Guan, Y., Perrine, C. L., Gerken, T. A., & Tabak, L. A. (2012). UDP-N-acetyl-α-D-galactosamine: polypeptide N-acetylgalactosaminyltransferases: completion of the family tree. *Glycobiology*, *22*(6), 768-777.

14. Ahuja, S., & Whorton, M. R. (2019). Structural basis for mammalian nucleotide sugar transport. *Elife*, *8*, e45221.

15. J. Ruan, H. Li, Z. Chen, A. Coghlan, L. J. M. Coin, Y. Guo, J. K. Hériché, Y. Hu, K. Kristiansen, R. Li, T. Liu, A. Moses, J. Qin, S. Vang, A. J. Vilella, A. Ureta-Vidal, L. Bolund, J. Wang, R. Durbin, TreeFam: 2008 update. *Nucleic Acids Res.* **36**(suppl_1), D735–D740 (2007).

16. M. J. Robertson, K. Kent, N. Tharp, K. Nozawa, L. Dean, M. Mathew, S. L. Grimm, Z. Yu, C. Légaré, Y. Fujihara, M. Ikawa, R. Sullivan, C. Coarfa, M.

M. Matzuk, T. X. Garcia, Large-scale discovery of male reproductive tract-specific genes through analysis of RNA-seq datasets. *BMC Biol*. **18**(1), 103 (2020). doi: 10.1186/s12915-020-00826-z PMID: 32814578

17. R. Wang, P. Zhang, J. Wang, Ma L, W. E, S. Suo, M. Jiang, J. Li, H. Chen, H. Sun, L. Fei, Z. Zhou, Y. Zhou, Y. Chen, W. Zhang, X. Wang, Y. Mei, Z. Sun, C. Yu, J. Shao, Y. Fu, Y. Xiao, F. Ye, X. Fang, H. Wu, Q. Guo, X. Fang, X. Li, X. Gao, D. Wang, P. F. Xu, R. Zeng, G. Xu, L. Zhu, L. Wang, J. Qu, D. Zhang, H. Ouyang, H. Huang, M. Chen, S. C. Ng, G. H. Liu, G. C. Yuan, G. Guo, X. Han, Construction of a cross-species cell landscape at single-cell level. *Nucleic Acids Res.* **51**(1), 501–516 (2022). https://doi.org/10.1093/nar/gkac633

18. J. Jumper, R. Evans, A. Pritzel, T. Green, M. Figurnov, O. Ronneberger, K. Tunyasuvunakool, R. Bates, A. Žídek, A. Potapenko, A. Bridgland, C. Meyer, S. A. A. Kohl, A. J. Ballard, A. Cowie, B. Romera-Paredes, S. Nikolov, R. Jain, J. Adler, T. Back, S. Petersen, D. Reiman, E. Clancy, M. Zielinski, M. Steinegger, M. Pacholska, T. Berghammer, S. Bodenstein, D. Silver, Vinyals. O, A. W. Senior, K. Kavukcuoglu, P. Kohli, D. Hassabis, Highly accurate protein structure prediction with AlphaFold. *Nature* **596**, 583–589 (2021). https://doi.org/10.1038/s41586-021-03819-2

19. K. D. Tsirigos, C. Peters, N. Shu, L. Käll, A. Elofsson, The TOPCONS web server for consensus prediction of membrane protein topology and signal peptides. *Nucleic Acids Res*. **43**(W1), W401–W407 (2015).

20. F. P. Kuhl, C. R. Giardina, Elliptic Fourier features of a closed contour. *Comput. Graph. Image Process.* **18**(3), 236–258 (1982).

21. D. Mashiko, M. Ikawa, K. Fujimoto, Mouse spermatozoa with higher fertilization rates have thinner nuclei. *PeerJ* **5**, e3913 (2017). https://doi.org/10.7717/peerj.3913

22. A. Morohoshi, H. Miyata, Y. Oyama, S. Oura, T. Noda, M. Ikawa, FAM71F1 binds to RAB2A and RAB2B and is essential for acrosome formation and male fertility in mice. *Development* **148**(21), dev199644 (2021).

23. H. Hasuwa, Y. Muro, M. Ikawa, N. Kato, Y. Tsujimoto, M. Okabe, Transgenic mouse sperm that have green acrosome and red mitochondria allow visualization of sperm and their acrosome reaction in vivo. *Exp. Anim.* **59**(1), 105–107 (2010).

24. Y. N. Lin, A. Roy, W. Yan, K. H. Burns, M. M. Matzuk, Loss of zona pellucida binding proteins in the acrosomal matrix disrupts acrosome biogenesis and sperm morphogenesis. *Mol. Cell Biol.* **27**(19), 6794–6805 (2007).

25. R. Yao, C. Ito, Y. Natsume, Y. Sugitani, H. Yamanaka, S. Kuretake, K. Yanagida, A. Sato, K. Toshimori, T. Noda, Lack of acrosome formation in mice lacking a Golgi protein, GOPC. *Proc. Natl. Acad. Sci. U. S. A.* **99**, 11211–11216 (2002).

26. Y. Fujihara, Y. Satouh, N. Inoue, A. Isotani, M. Ikawa, M. Okabe, SPACA1-deficient male mice are infertile with abnormally shaped sperm heads reminiscent of globozoospermia. *Development* **139**(19), 3583–3589 (2012).

27. E. Kim, M. Yamashita, T. Nakanishi, K. E. Park, M. Kimura, S. I. Kashiwabara, T. Baba, Mouse sperm lacking ADAM1b/ADAM2 fertilin can fuse with the egg plasma membrane and effect fertilization. *J. Biol. Chem.* **281**(9), 5634–5639 (2006).

28. Y. Fujihara, A. Oji, K. Kojima-Kita, T. Larasati, M. Ikawa, Co-expression of sperm membrane proteins CMTM2A and CMTM2B is essential for

ADAM3 localization and male fertility in mice. *J. Cell Sci.* **131**(19), jcs221481 (2018).
29. R. Shamsadin, I. M. Adham, K. Nayernia, U. A. Heinlein, H. Oberwinkler, W. Engel, Male mice deficient for germ-cell cyritestin are infertile. *Biol. Reprod.* **61**(6), 1445–1451 (1999).
30. R. Yamaguchi, Y. Muro, A. Isotani, K. Tokuhiro, K. Takumi, I. Adham, M. Ikawa, M. Okabe, Disruption of ADAM3 impairs the migration of sperm into oviduct in mouse. *Biol. Reprod.* **81**(1), 142–146 (2009).
31. Y. Fujihara, K. Tokuhiro, Y. Muro, G. Kondoh, Y. Araki, M. Ikawa, M. Okabe, Expression of TEX101, regulated by ACE, is essential for the production of fertile mouse spermatozoa. *Proc. Natl. Acad. Sci.* **110**(20), 8111–8116 (2013).
32. J. H. Krege, S. W. John, L. L. Langenbach, J. B. Hodgin, J. R. Hagaman, E. S. Bachman, J. C. Jennette, D. A. O'Brien, O. Smithies, Male-female differences in fertility and blood pressure in ACE-deficient mice. *Nature* **375**,146–148 (1995). doi: 10.1038/375146a0.
33. J. R. Hagaman, J. S. Moyer, E. S. Bachman, M. Sibony, P. L. Magyar, J. E. Welch, O. Smithies, J. H. Krege, D. A. O'Brien, Angiotensin-converting enzyme and male fertility. *Proc. Natl. Acad. Sci. U. S. A.* **95**, 2552–2557 (1998). doi: 10.1073/pnas.95.5.2552.
34. R. Yamaguchi, K. Yamagata, M. Ikawa, S. B. Moss, M. Okabe, Aberrant distribution of ADAM3 in sperm from both angiotensin-converting enzyme (Ace)—and calmegin (Clgn)-deficient mice. *Biol. Reprod.* **75**, 760–766 (2006). doi: 10.1095/biolreprod.106.052977
35. Y. Fujihara, M. Okabe, M. Ikawa, GPI-anchored protein complex, LY6K/TEX101, is required for sperm migration into the oviduct and male fertility in mice. *Biol. Reprod.* **90**(3), 60–61 (2014).
36. Y. Fujihara, S. Herberg, A. Blaha, K. Panser, K. Kobayashi, T. Larasati, M. Novatchkova, H. C. Theussl, O. Olszanska, M. Ikawa, A. Pauli, The conserved fertility factor SPACA4/Bouncer has divergent modes of action in vertebrate fertilization. *Proc. Natl. Acad. Sci. U. S. A.* **118**(39), e2108777118 (2021).
37. Y. Fujihara, T. Noda, K. Kobayashi, A. Oji, S. Kobayashi, T. Matsumura, T. Larasati, S. Oura, K. Kojima-Kita, Z. Yu, M. M. Matzuk, M. Ikawa, Identification of multiple male reproductive tract-specific proteins that regulate sperm migration through the oviduct in mice. *Proc. Natl. Acad. Sci. U. S. A.* **116**(37), 18498–18506 (2019).
38. N. Inoue, M. Ikawa, A. Isotani, M. Okabe, The immunoglobulin superfamily protein Izumo is required for sperm to fuse with eggs. *Nature* **434**(7030), 234–238 (2005).
39. K. Toshimori, S. Araki, I. Tanii, C. Ōura, Masking the cryptodeterminant on the 54-kilodalton mouse sperm surface antigen. *Biol. Reprod.* **47**(6), 1161–1167 (1992).
40. T. Noda, Y. Lu, Y. Fujihara, S. Oura, T. Koyano, S. Kobayashi, M. M. Matzuk, M. Ikawa, Sperm proteins SOF1, TMEM95, and SPACA6 are required for sperm− oocyte fusion in mice. *Proc. Natl. Acad. Sci. U. S. A.* **117**(21), 11493–11502 (2020).
41. D. Bojar, L. Meche, G. Meng, W. Eng, D. F. Smith, R. D. Cummings, L. K. Mahal, A useful guide to lectin binding: machine-learning directed annotation of 57 unique lectin specificities. *ACS Chem. Biol.* **17**(11), 2993–3012 (2022).

42. S. Chen, L. C. Francioli, J. K. Goodrich, R. L. Collins, M. Kanai, Q. Wang, J. Alföldi, N. A. Watts, C. Vittal, L. D. Gauthier, T. Poterba, M. W. Wilson, Y. Tarasova, W. Phu, M. T. Yohannes, Z. Koenig, Y. Farjoun, E. Banks, S. Donnelly, S. Gabriel, N. Gupta, S. Ferriera, C. Tolonen, S. Novod, L. Bergelson, D. Roazen, V. Ruano-Rubio, M. Covarrubias, C. Llanwarne, N. Petrillo, G. Wade, T. Jeandet, R. Munshi, K. Tibbetts, A. O'Donnell-Luria, M. Solomonson, C. Seed, A. R. Martin, M. E. Talkowski, H. L. Rehm, M. J. Daly, G. Tiao, B. M. Neale, D. G. MacArthur, K. J. Karczewski, gnomAD Project Consortium, A genome-wide mutational constraint map quantified from variation in 76,156 human genomes. *bioRxiv* **2022-03**, PPR556342 (2022). https://doi.org/10.1101/2022.03.20.485034

43. J. Cheng, G. Novati, J. Pan, C. Bycroft, A. Žemgulytė, T. Applebaum, A. Pritzel, L. H. Wong, M. Zielinski, T. Sargeant, R. G. Schneider, A. W. Senior, J. Jumper, D. Hassabis, P. Kohli, Ž. Avsec, Accurate proteome-wide missense variant effect prediction with AlphaMissense. *Science* **381**(6664), eadg7492 (2023).

44. I. A. Adzhubei, S. Schmidt, L. Peshkin, V. E. Ramensky, A. Gerasimova, P. Bork, A. S. Kondrashov, S. R. Sunyaev. *Nat Methods* **7**(4), 248–249 (2010).

45. JM. Bedford . Effects of elevated temperature on the epididymis and testis: experimental studies. Adv Exp Med Biol. 1991;286:19-32. doi: 10.1007/978-1-4684-5913-5_3. PMID: 2042501.

46. M. Aebi, N-linked protein glycosylation in the ER. *Biochim. Biophys. Acta* **1833**(11), 2430–2437 (2013).

47. Wang, H., Iida-Norita, R., Mashiko, D., Pham, A. H., Miyata, H., & Ikawa, M. (2024). Golgi associated RAB2 interactor protein family contributes to murine male fertility to various extents by assuring correct morphogenesis of sperm heads. *PLoS Genetics*, *20*(6), e1011337.

48. Martinez, G., Coutton, C., Loeuillet, C., Cazin, C., Muroňová, J., Boguenet, M., ... & Arnoult, C. (2022). Oligogenic heterozygous inheritance of sperm abnormalities in mouse. *Elife*, *11*, e75373.

49. Fujihara, Y., Miyata, H., & Ikawa, M. (2018). Factors controlling sperm migration through the oviduct revealed by gene-modified mouse models. *Experimental Animals*, *67*(2), 91-104.

50. D. Wang, L. Cheng, W. Xia, X. Liu, Y. Guo, X. Yang, X. Guo, E. Y. Xu, LYPD4, mouse homolog of a human acrosome protein, is essential for sperm fertilizing ability and male fertility. *Biol. Reprod.* **102**(5), 1033–1044 (2020).

51. N. Inoue, M. Ikawa, M. Okabe, Putative sperm fusion protein IZUMO and the role of N-glycosylation. *Biochem. Biophys. Res. Commun.* **377**, 910–914 (2008)

52. Kotaja, N., Kimmins, S., Brancorsini, S., Hentsch, D., Vonesch, J. L., Davidson, I., ... & Sassone-Corsi, P. (2004). Preparation, isolation and characterization of stage-specific spermatogenic cells for cellular and molecular analysis. *Nature methods*, *1*(3), 249-254.

53. Y. Toyoda, M. Yokoyama, T. Hosi, Studies on the fertilization of mouse eggs in vitro. *Jpn. J. Anim. Reprod.* **16**, 152–157 (1971). 10.1262/jrd1955.16.152

54. H. Miyata, Y. Satouh, D. Mashiko, M. Muto, K. Nozawa, K. Shiba, Y. Fujihara, A. Isotani, K. Inaba, M. Ikawa, Sperm calcineurin inhibition prevents

mouse fertility with implications for male contraceptive. *Science*, **350**(6259), 442–445 (2015).

55. H. Niwa, K. Yamamura, J. Miyazaki, Efficient selection for high-expression transfectants with a novel eukaryotic vector. *Gene* **108**, 193–199 (1991). 10.1016/0378-1119(91)90434-D

56. G. Tiscornia, O. Singer, I. M. Verma, Production and purification of lentiviral vectors. *Nat. Protoc.* **1**, 241–245 (2006). 10.1038/nprot.2006.37

57. K. Shimada, S. Park, H. Miyata, Z. Yu, A. Morohoshi, S. Oura, M. M. Matzuk, M. Ikawa, ARMC12 regulates spatiotemporal mitochondrial dynamics during spermiogenesis and is required for male fertility. *Proc. Natl. Acad. Sci. U. S. A.* **118**, e2018355118 (2021). 10.1073/pnas.2018355118

58. M. Postma, J. Goedhart, PlotsOfData—A web app for visualizing data together with their summaries. *PLoS Biol.* **17**(3), e3000202 (2019).

Acknowledgments

We express our sincere gratitude to Ms. Saki Nishioka and the NPO for Biotechnology Research and Development for their valuable technical support and to the members of both the Department of Experimental Genome Research and Animal Resource Center for Infectious Diseases at the Research Institute for Microbial Diseases (RIMD) of Osaka University, Japan for their assistance and engaging discussions during the experiments. We acknowledge the RIMD NGS core facility for its valuable support in sequencing and data analysis. We also thank A. Ninomiya and F. Sugihara for MS analysis (RIMD Core Instrumentation Facility).

Funding: This work was financially supported by the Ministry of Education, Culture, Sports, Science and Technology/Japan Society for the Promotion of Science (JP21K19569 and JP22H03214 to H.M.; JP21H05033, JP22H04922 and JP23K20043 to M.I.); the Japan Science and Technology Agency (JPMJFR211F to H.M.; JPMJCR21N1 to M.I.); the Japan Agency for Medical Research and Development (JP23jf0126001, JP23fa627002, and JP23fa627006 to M.I.); the Takeda Science Foundation (grants to H.M. and M.I.); the *Eunice Kennedy Shriver* National Institute of Child Health and Human Development (R01HD088412 to M.M and M.I.); and the Bill & Melinda Gates Foundation (INV-001902 to M.M. and M.I.). OU master plan (JPMXP1323015484 to M.I.)

Data and material availability: All data needed to evaluate the conclusions in the paper are present in the paper and/or the Supplementary Materials. The gene-manipulated mouse lines used in this study were deposited at the RIKEN BioResource Research Center (RIKEN BRC, Tsukuba, Japan) and the Center for Animal Resources and Development (CARD) Kumamoto University (Kumamoto, Japan). These cell lines are available through these centers subject to scientific review and completion of a material transfer agreement. Requests for access to genetically manipulated mice should be submitted to these centers.

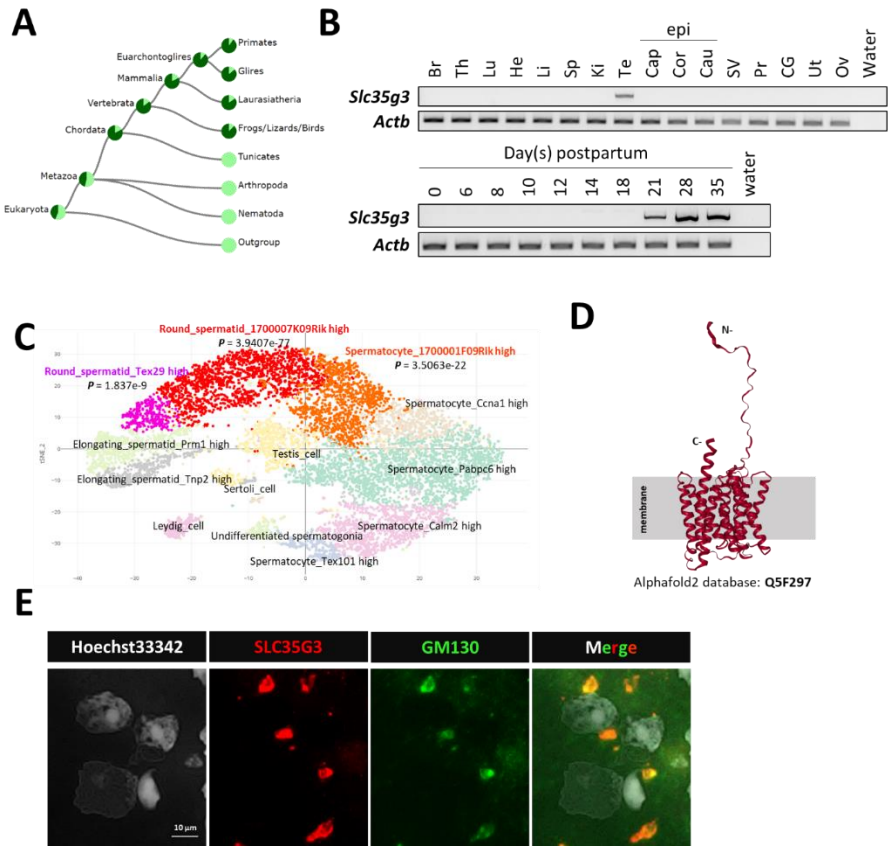

Fig. 1. SLC35G3 is a multi-pass transmembrane protein with unique testes-specific expression in the Golgi apparatus during early spermiogenesis.
(A) Phylogenetic tree of *Slc35g3* from the TreeFam database, with dark green areas indicating the presence and light green areas indicating the absence of *Slc35g3*. **(B)** RT-PCR results across multiple tissues (upper panel) and from testes at various days postpartum (lower panel); Br: brain, Th: thymus, Lu: lung, He: heart, Li: liver, Sp: spleen, Ki: kidney, Te: testis; Epi: epididymis, Cap: caput epididymis, Cor: corpus epididymis, Cau: cauda epididymis; SV: seminal vesicle, Pr: prostate, CG: coagulating gland, Ut: uterus, Ov: ovary. β-actin (Actb) was used as the loading control. **(C)** scRNA-seq prediction of cells strongly expressing *Slc35g3* mRNA (Mouse cell atlas). Dots with low transparency represent cells with predicted expression. **(D)** SLC35G3 structure predicted using Alpha Fold. **(E)** From left to right: Hoechst33342 staining image, SLC35G3 immunostaining image, GM130 immunostaining image, and merged image of wild-type testicular germ cells. Scale bar: 10 µm

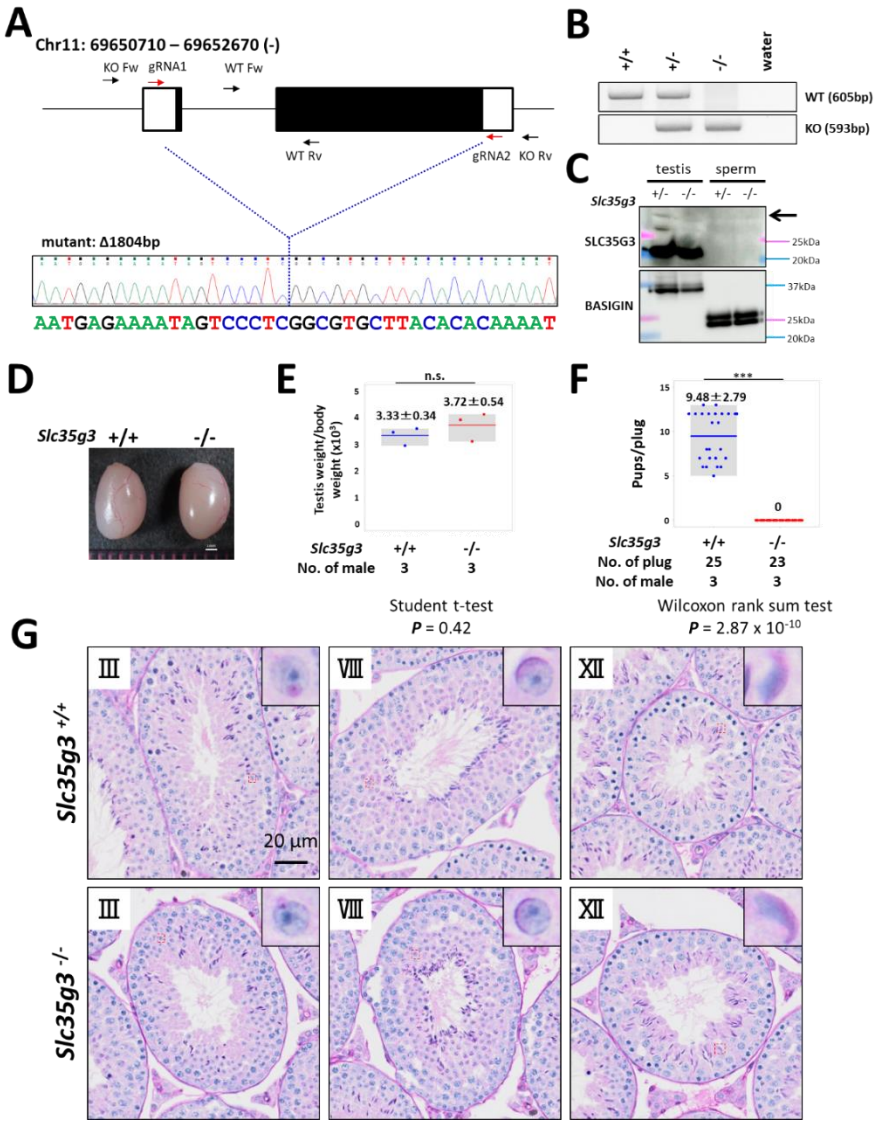

Fig. 2. *Slc35g3*$^{-/-}$ induces male sterility.
(A) Depiction of *Slc35g3* gene location and structure, gRNA/primer design, and the sequencing result of the mutant (deleted) allele. **(B)** PCR genotyping results for *Slc35g3*$^{+/+}$, *Slc35g3*$^{+/-}$, *Slc35g3*$^{-/-}$, and water are presented. **(C)** Western blot analysis results obtained with *Slc35g3*$^{+/-}$ and *Slc35g3*$^{-/-}$ testis lysates and *Slc35g3*$^{+/-}$ and *Slc35g3*$^{-/-}$-derived cauda epididymal sperm lysates are shown. **(D, E)** Similar testis sizes (D) and weights (E) from *Slc35g3*$^{+/+}$ and *Slc35g3*$^{-/-}$ mice (two-sided Student's t-test; $P = 0.42$). **(F)** Comparison of the number of pups per vaginal plug between *Slc35g3*$^{+/+}$ and *Slc35g3*$^{-/-}$ mice (Wilcoxon rank-sum test; $P = 2.87 \times 10^{-10}$. **(G)** Histological analysis of testis sections from *Slc35g3*$^{+/+}$ mice (upper panels) and those from *Slc35g3*$^{-/-}$ mice (lower panels); images depict stages III (Golgi phase), VIII (acrosome phase), and XII (maturation phase).

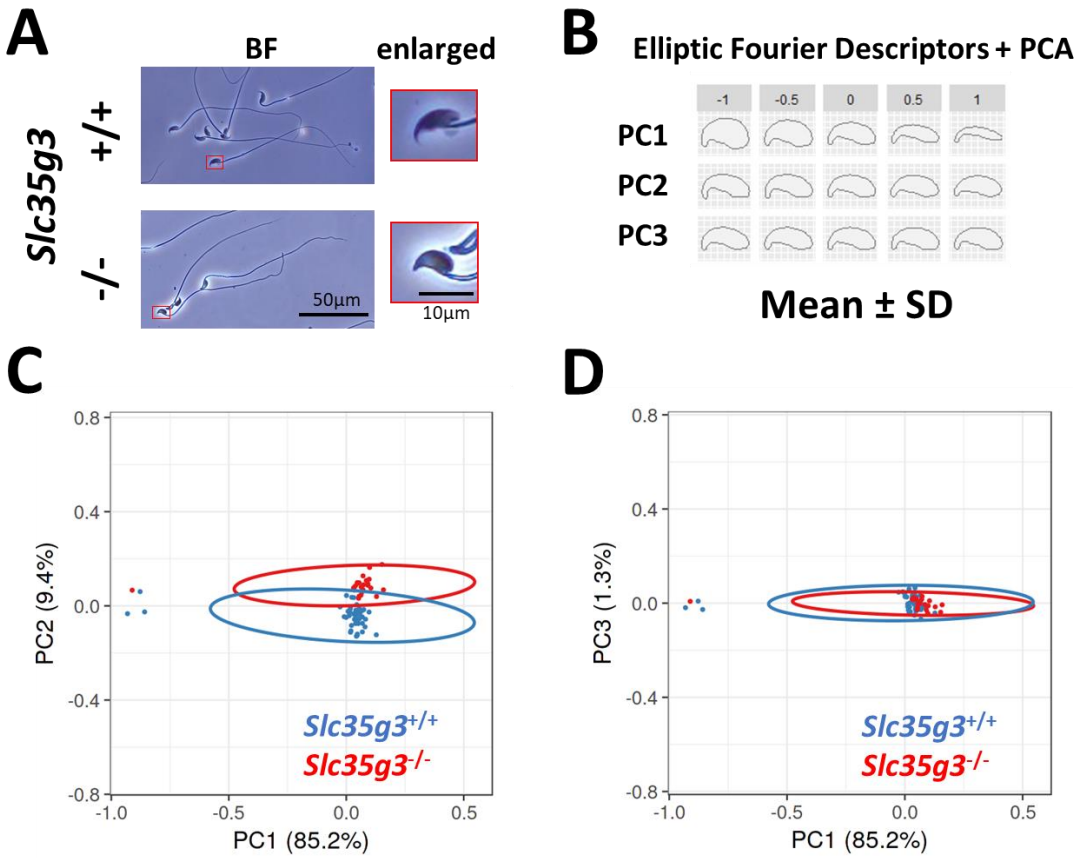

Fig. 3. *Slc35g3* is essential for sperm head formation.
(A) Bright-field (BF) views of *Slc35g3*$^{+/+}$-derived sperm (upper panels) versus *Slc35g3*$^{-/-}$-derived sperm (lower panels); red frames are images enlarged four times. Scale bar: 50 µm for BF images, 10 µm for enlarged ones. **(B)** Morphological characteristics are indicated by mean ± SD of each principal component (PC) following elliptic Fourier analysis; the upper value represents SD, with zero indicating average morphology. **(C, D)** Plots of PC1-PC2 (C) and PC1-PC3 (D) coordinates of the elliptic Fourier analysis of sperm from *Slc35g3*$^{+/+}$ mice (blue encircled) versus *Slc35g3*$^{-/-}$ mice (red encircled); circles represent 95% confidence ellipses. Scale bar = 10 µm.

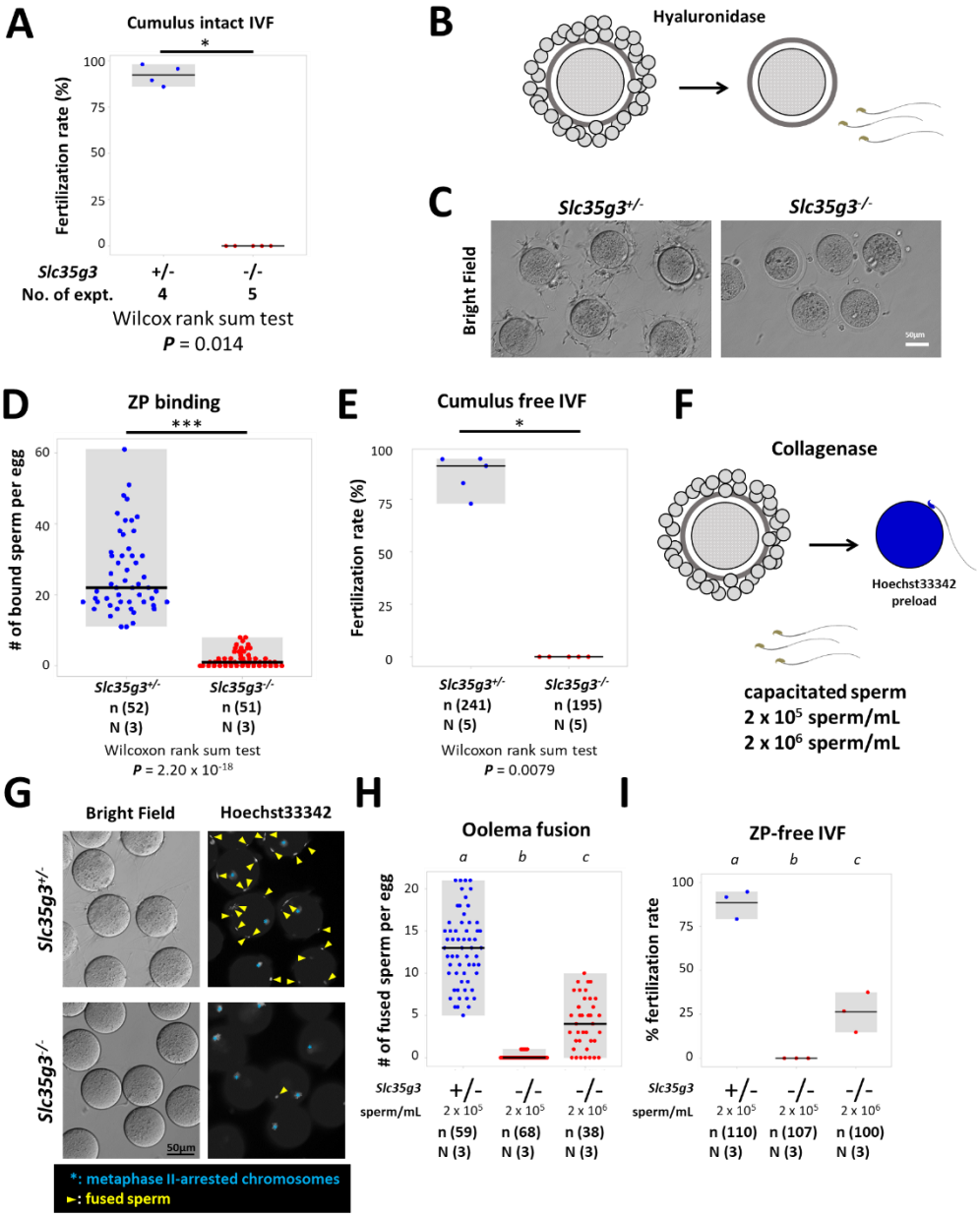

Fig. 4. *Slc35g3*$^{-/-}$-derived spermatozoa are defective in ZP binding and oolemma fusion.

(A) The IVF fertilization rate of cumulus-intact oocytes using *Slc35g3*$^{+/-}$ and *Slc35g3*$^{-/-}$ -derived sperm. Wilcoxon rank-sum test $P = 0.014$. (B) Outline of the procedure of cumulus cell-free IVF. (C) *Slc35g3*$^{+/-}$-derived and *Slc35g3*$^{-/-}$-derived sperm binding to cumulus-free oocytes after insemination. Scale bar = 50 µm. (D) The number of bound sperm per egg for *Slc35g3*$^{+/-}$-derived and *Slc35g3*$^{-/-}$-derived sperm (Wilcoxon rank-sum test $P = 2.20 \times 10^{-18}$). (E) The fertilization rate of cumulus cell-free IVF using Slc35g3$^{+/-}$-derived and Slc35g3$^{-/-}$-derived sperm. (F) The procedure of ZP-free IVF. Wilcoxon rank-sum test; $\boldsymbol{P} = 0.0079$. (G) Brightfield and Hoechst33342 staining of oocytes and

Slc35g3$^{+/-}$-derived and *Slc35g3*$^{-/-}$-derived sperm after insemination into ZP-free oocytes; Yellow arrowheads indicate fused spermatozoa and light blue asterisks indicate metaphase II-arrested chromosomes. (H) The number of fused sperm per egg using *Slc35g3*$^{+/-}$-derived and *Slc35g3*$^{-/-}$-derived sperm (2×10^5 sperm/mL and 2×10^6 sperm/mL, respectively). Significant differences are indicated by distinct symbols. (I) The fertilization rate of ZP-free IVF using *Slc35g3*$^{+/-}$-derived and *Slc35g3*$^{-/-}$-derived sperm (2×10^5 sperm/mL and 2×10^6 sperm/mL, respectively). Significant differences are indicated by distinct symbols.

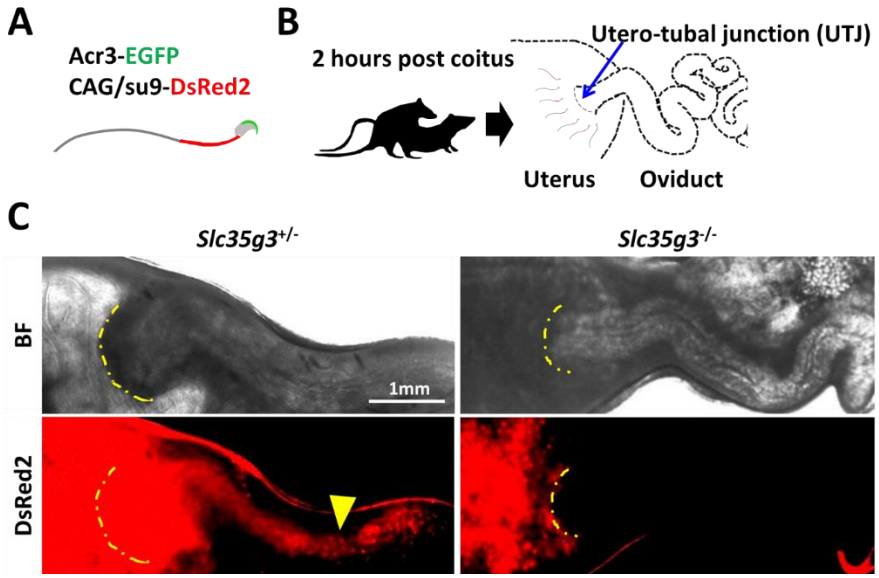

Fig. 5. *Slc35g3*-deficient mice show impaired sperm migration to the oviduct
(A) Illustration of Tg (CAG/su9-DsRed2, Acr3-eGFP) sperm. **(B)** A schematic diagram of the sperm migration assay. **(C)** Bright field (top panel) and Dsred2 (bottom panel) images of the uteri and oviducts of females after mating with control *Slc35g3*$^{+/-}$and *Slc35g3*$^{-/-}$ male mice. The yellow dashed line indicates the uterotubal junction (UTJ), and the yellow arrowhead represents the sperm from control *Slc35g3*$^{+/-}$ male mice that have traversed the UTJ.

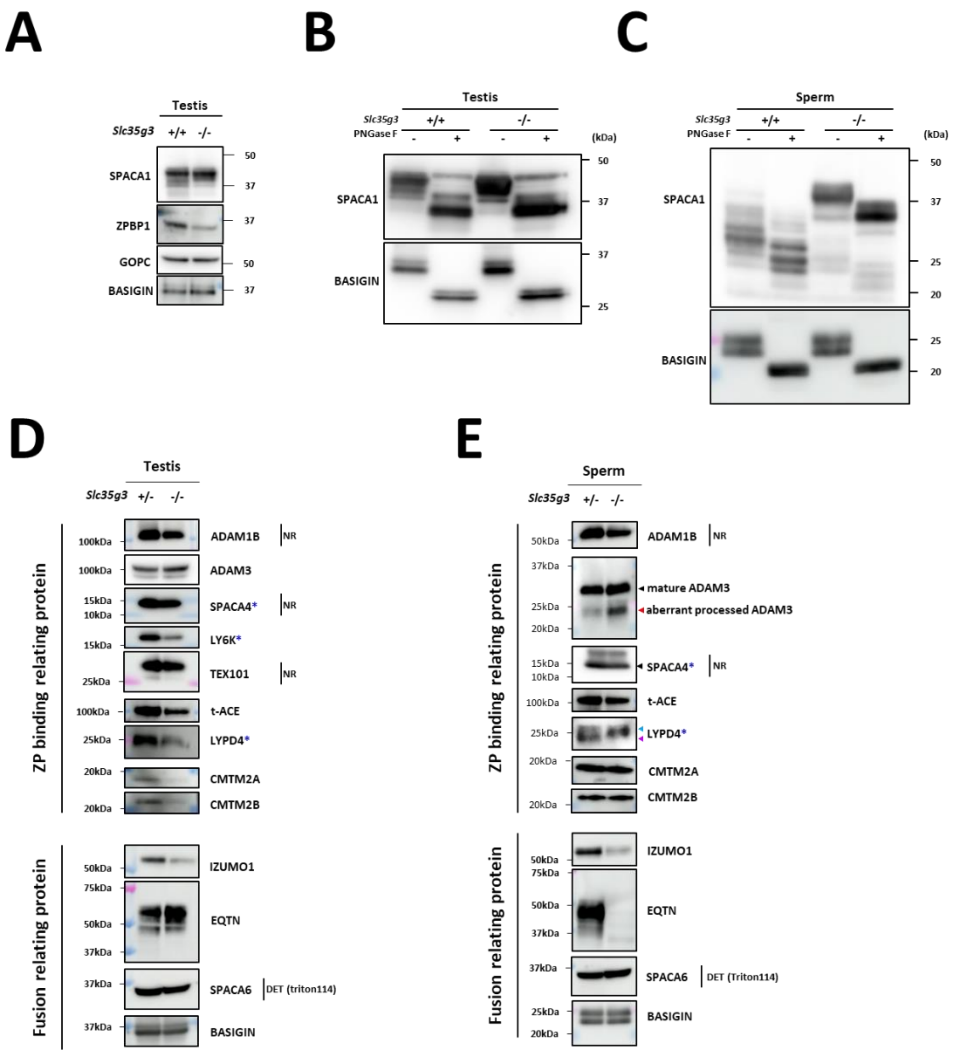

Fig. 6. Disruption of *Slc35g3* leads to its reduced testicular expression and abnormal processing of multiple sperm proteins

(A) Western blot analyses of SPACA1, ZPBP1, and GOPC in *Slc35g3*$^{+/+}$ and *Slc35g3*$^{-/-}$ testes, with BASIGIN used as a loading control. **(B)** Western blot analysis of PNGaseF treated or non-treated SPACA1 in *Slc35g3*$^{+/+}$ and *Slc35g3*$^{-/-}$ testes, with BASIGIN used as a loading control. **(C)** Western blot analysis of PNGaseF treated or non-treated SPACA1 in *Slc35g3*$^{+/+}$-derived and *Slc35g3*$^{-/-}$-derived spermatozoa, with BASIGIN used as a loading control. **(D)** Western blot analyses of ADAM1B, ADAM3, SPACA4, LY6K, TEX101, t-ACE, LYPD4, CMTM2A, CMTM2B, IZUMO1, EQTN, and SPACA6 in *Slc35g3*$^{+/-}$ and *Slc35g3*$^{-/-}$ testes, with BASIGIN used as a loading control. All protein samples were processed under reducing and denaturing conditions unless otherwise specified. Non-reducing and non-denaturing conditions are denoted as NR. For SPACA6 detection, fractions of testis proteins from wild-type and knockout specimens, extracted using Triton X-114, were utilized (abbreviated as DET). Genes marked with blue asterisks show reduced ZP binding upon knockout, whereas ADAM3 remains unaffected. **(E)** Western blot analyses of ADAM1B, ADAM3, SPACA4, t-ACE, LYPD4, CMTM2A,

CMTM2B, IZUMO1, EQTN, and SPACA6 in *Slc35g3*$^{+/+}$-derived and *Slc35g3*$^{-/-}$-derived spermatozoa, BASIGIN used as a loading control. The black arrowhead indicates the predicted protein size, whereas the red arrowhead indicates an aberrantly processed protein isoform. Additionally, the light blue and purple arrowheads mark the two bands observed in the wild-type sample.

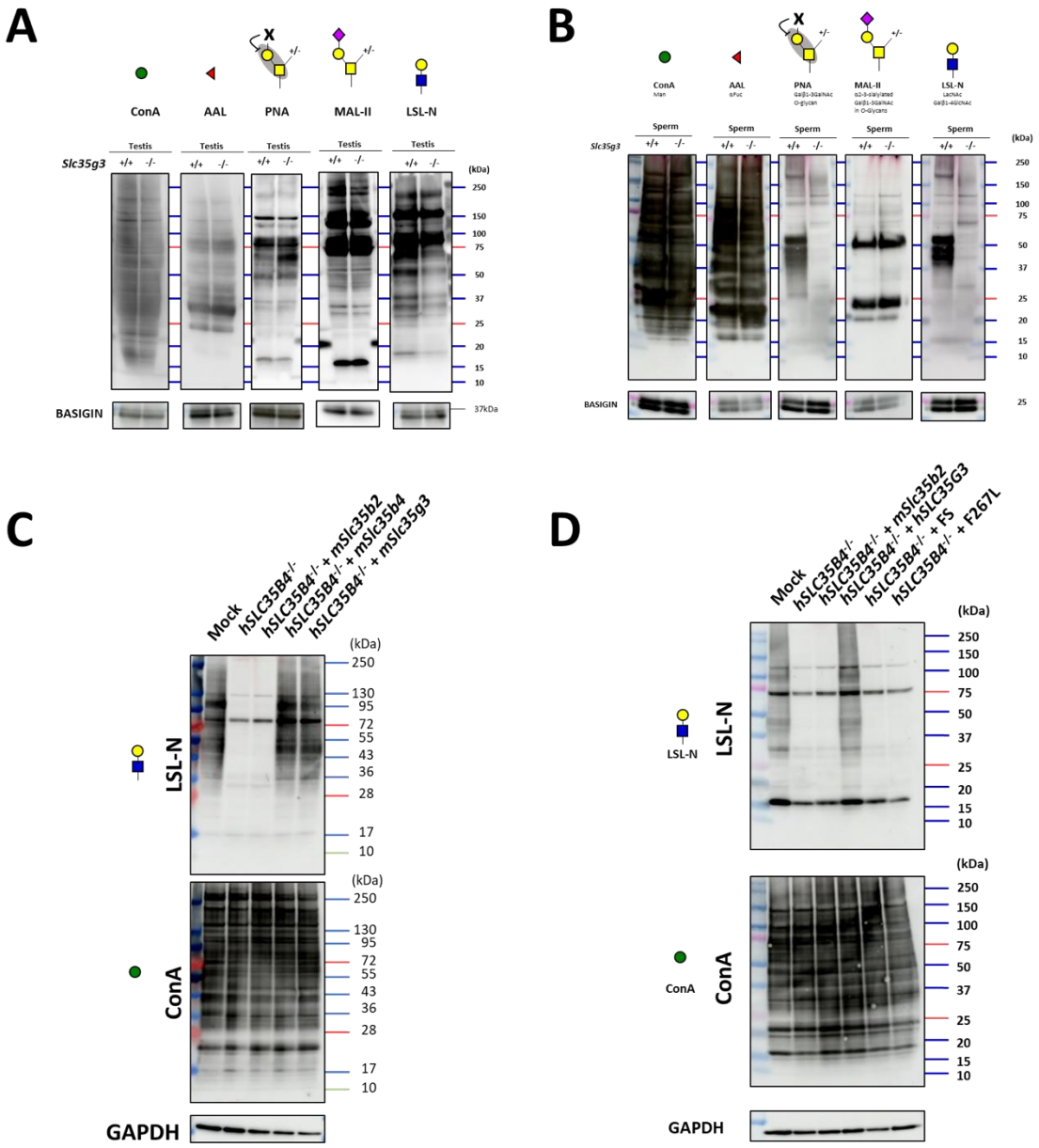

Fig. 7. *Slc35g3*$^{-/-}$ testis showed impaired glycan structure
(A) Lectin blot (LB) analyses using ConA, AAL, PNA, MAL-II, and LSL-N in *Slc35g3*$^{+/+}$ and *Slc35g3*$^{-/-}$ testes, BASIGIN as a loading control. Green circles represent mannose, red

triangles fucose, yellow squares GalNAc, yellow circles galactose, purple diamonds sialic acid, and blue squares GlcNAc. **(B)** LB analyses using ConA, AAL, PNA, MAL-II, and LSL-N in *Slc35g3*$^{+/+}$ and *Slc35g3*$^{-/-}$ derived spermatozoa. **(C)** LB analyses of LSL-N and ConA in SLC35B4 deficient HEK293T cells, with GAPDH as a loading control. mSlc35b2, mSlc35b4 and mSlc35g3 were expressed in SLC35B4 deficient cells. **(D)** LB analyses of LSL-N and ConA in hSLC35G3 mutant transfected SLC35B4 deficient cells, with GAPDH, were used as a loading control. FS: T179HfsTer27.